Eigenfrequency Shift Mechanism due to an Interior Blockage in a Pipe

Moez Louati[1] and Mohamed S. Ghidaoui[2]

Abstract: The presence of blockages in water supply systems wastes energy, decreases system performance, and may pose safety concerns. Previous research showing that blockages induce a shift in the resonant frequencies (eigenfrequencies) of the pipe system made use of that shift information to develop improved inverse problem solution techniques for blockage detection. This paper studies in more detail the eigenfrequency shift mechanism itself that arises from an interior blockage in a pipe system, and shows that more information could be obtained from understanding the nature and physical basis for the shift mechanism. This improved understanding can improve the computational efficiency of current blockage detection solution techniques. This paper explains the mechanism causing positive, negative, and zero eigenfrequency shifts, and shows how these shifts vary with blockage location, size, and resonant modes. Zero shift occurs if the midlength of the blockage is located at a position where the pressure head and flow harmonics are equal in magnitude, whereas maximum (or significant) shifts occur if the midlength of the blockage is located at either a pressure node (if the shift is negative) or a stagnation point (if the shift is positive), where pressure node and stagnation points are where the pressure and flow harmonics' magnitudes are zero. It is also shown that the Bragg resonance phenomenon directly influences the direction and magnitude of the observed eigenfrequency under different resonant modes. **DOI: 10.1061/(ASCE)HY.1943-7900.0001380.**

Author keywords: Unsteady pipe flow; Eigenfrequency shift mechanism; Wave-blockage interaction; Bragg resonance; Blockage detection.

Introduction

During their lifetime, pressurized conduits transporting liquids such as freshwater, seawater, sanitary and stormwater, oil, and blood may develop full or partial blockage at discrete locations or distributed over considerable lengths of the affected pipeline. The blockages are due to reduction in pipe cross-sectional area caused by various physical and/or chemical processes. Blockages waste energy and financial resources by reducing pipe carrying capacity and can increase the potential for in-pipe liquid contamination (e.g., James and Shahzad 2012). Reduced flow area in severely blocked pipes may also throttle flow to such a degree that flow is redistributed in a pipe network, resulting in a reduction of system redundancy (reliability) or overpressure of some pipes in the system, thereby increasing leakage. Increases in leakage and energy consumed to pump the liquid through reduced pipe cross-sectional areas also means that the energy footprint of the pipe system is increased, adding to environmental problems of air pollution and greenhouse gas emissions (e.g., Coelho and Andrade-Campos 2014). Consequently, it is important to be able to quickly and reliably detect and characterize the severity and location of pipe blockage so that it may be dealt with in a timely manner. Early detection of developing blockage would also lead to more optimal rehabilitation and replacement programs that minimize lifetime costs associated with pipe blockage.

A well-known approach from the field of acoustic phonetics (Stevens 1998; Fant 1975; Heinz 1967; Mermelstein 1967; Schroeder 1967) uses measured transient pressure(s) at one or more monitored locations in a pipe or conduit to infer the internal shape of the conduit. This technique is used to image the human vocal tract system. More recently, the technique elicited considerable interest on the part of water supply researchers (Duan et al. 2011, 2013; Lee et al. 2013;) and its utility was extended to other fields of application (Duan et al. 2015).

Some of this research shows that eigenfrequencies of a measured pressure signal vary with cross-sectional area of a conduit (e.g., Duan et al. 2011; De Salis and Oldham 1999; Stevens 1998; Schroeter and Sondhi 1994; Qunli and Fricke 1990, 1989; Milenkovic 1987, 1984; Sondhi and Resnick 1983; Domis 1980, 1979; Fant 1975; Sondhi and Gopinath 1971; Heinz 1967; Mermelstein 1967; Schroeder 1967). This dependence between eigenfrequencies and conduit cross-sectional area has recently been used to formulate algorithms for defect detection in water supply systems (WSSs) (e.g., Louati and Ghidaoui 2015; Duan et al. 2011, 2013; Lee et al. 2008, 2013; Louati 2013; Meniconi et al. 2013; Sattar et al. 2008; Mohapatra et al. 2006; Wang et al. 2005).

The economic and hydraulic consequences of blockages in pipelines led to an emphasis in research to develop detection algorithms for blockages. Accordingly, the focus of past research is primarily on the inverse problem where mathematical relations linking eigenfrequencies to the cross-sectional area of the pipe are formulated, and algorithms for using these relationships to infer blockages from measured eigenfrequencies are proposed (e.g., Duan et al. 2013, 2011; Lee et al. 2013; Meniconi et al. 2013). While this research direction is promising and has led to proof of concept under idealized laboratory settings, there are several unresolved issues. For example, there is neither a proof that the inverse problem,

[1]Postdoctoral Fellow, Dept. of Civil and Environmental Engineering, School of Engineering, Hong Kong Univ. of Science and Technology, Kowloon, Hong Kong (corresponding author). E-mail: mlouati@connect.ust.hk

[2]Chair Professor, Dept. of Civil and Environmental Engineering, School of Engineering, Hong Kong Univ. of Science and Technology, Kowloon, Hong Kong. E-mail: ghidaoui@ust.hk

Note. This manuscript was submitted on October 16, 2016; approved on May 30, 2017; published online on October 26, 2017. Discussion period open until March 26, 2018; separate discussions must be submitted for individual papers. This paper is part of the ***Journal of Hydraulic Engineering***, © ASCE, ISSN 0733-9429.

which relates the unknown blockage properties to the measured eigenfrequencies, has a unique solution nor is there a technique to find it even if it exists. In fact, current solutions of this inverse problem in the water supply field require that the number of blockages is known a priori (e.g., Duan et al. 2013; Lee et al. 2013), which is unrealistic in practice. In addition, the computational time needed to solve the inverse problem grows almost exponentially with the number of blockages.

In the field of vocal tract geometric characterization, which is governed by the same general wave equations as the problem of blockage detection in pipes, progress has been made instead by improving understanding of the forward problem and using this improved understanding to develop more efficient and robust inversion techniques. For example, Schroeder (1967) showed that the eigenfrequency shift of the mth pressure mode is directly linked to the amplitude of the mth term in the Fourier series expansion of the cross-sectional area function of the conduit with respect to longitudinal distance. He showed how this relationship can be imposed as a constraint that guarantees uniqueness of the inverse problem. In addition, Schroeder (1967) showed that the Ehrenfest theorem (Ehrenfest 1917) can be used to formulate an algorithm for determining the geometry of the vocal tract from measured values of the eigenfrequencies of the acoustic pressure wave. Schroeder's (1967) results formed the basis for several robust algorithms to solve the inverse problem in the vocal tract field (e.g., De Salis and Oldham 1999; Stevens 1998; Schroeter and Sondhi 1994; Qunli and Fricke 1990, 1989; Milenkovic 1987, 1984; Sondhi and Resnick 1983; Domis 1980, 1979; Fant 1975; Sondhi and Gopinath 1971). El-Rahed and Wagner (1982) investigated the forward problem of blockage–acoustic wave interaction in finite cylindrical cavities and concluded that one-dimensional wave theory is acceptable for determining large blockage, while three-dimensional analysis is only needed to reveal the details of the acoustic field.

Louati and Ghidaoui (2016) provide an in-depth study of the eigenfrequency shift mechanism for the case of blockage at a boundary. For the case of a shallow blockage (i.e., small radial protrusion), Louati and Ghidaoui (2016) derived an equation for the eigenfrequency shift based on the work done by the radiation pressure (Borgnis 1953; Beyer 1978; Louati and Ghidaoui 2016; Schroeder 1967). They showed that the shift for the shallow blockage case is governed by the change in work done at the blockage boundaries. Louati et al. (2016) studied the case of internal blockage in a reservoir-pipe-valve (RPV) system and showed that changes in the magnitude of the shift is governed by Bragg resonance phenomena (Bragg and Bragg 1913; Mei 1985; Louati 2013, 2016).

This paper extends the understanding of the blockage phenomenon and its effect on key aspects of the governing wave equations to shed greater light on the forward problem. The eigenfrequency shift mechanism is analyzed and studied in some detail and rigor because it is a key component of the forward problem that must be understood if one hopes to address difficult issues that arise in connection with its inversion. This paper explains the nature of the mechanism causing positive, negative, and zero eigenfrequency shifts, and describes how this shift varies with blockage location, size, and resonant modes. This understanding is essential to improve the accuracy and convergence of inverse solution techniques for transient-based defect detection methods (TBDDMs) and pipe cross-section characterization. The theoretical model considered in this work is for a RPV system containing a single interior blockage.

The paper is organized in the following manner: first, the problem statement is formulated. Then the shift mechanism for the case of a shallow blockage is described using the radiation pressure equation derived in Louati and Ghidaoui (2016). Then the effects of severe and moderate blockages on the shift behavior are discussed in detail. Finally, some conclusions are drawn.

Problem Statement

For the purposes of this paper, a RPV system is considered as shown schematically in Fig. 1. The blocked pipe system is modeled as a series of three pipes, with the interior pipe having a reduced (blocked) diameter. Two junction boundary conditions are also solved, one at each end of the interior pipe where it connects with the upstream and downstream pipes, respectively. The three pipes are defined as Pipe 1 with length l_1 and cross-sectional area $A_1 = A_0$, Pipe 2 with length l_2 and cross-sectional area $A_2 < A_0$, and Pipe 3 with length l_3 and cross-sectional area $A_3 = A_0$, where A_0 is the intact cross-sectional area. Pipe 2 represents the blockage. The ratio between the cross-sectional area of the blocked and intact pipe is $\alpha = A_2/A_0$. The dimensionless lengths are defined by x/L, $\eta_1 = l_1/L$, $\eta_2 = l_2/L$, and $\eta_3 = l_3/L$, where $L = l_1 + l_2 + l_3$ is the total length of the blocked pipe system, and x is the distance along the pipe length from the reservoir (Fig. 1). The location of the midlength of the blockage is defined by $\eta_b = \eta_3 + \eta_2/2$. It is assumed that the pipe system is one-dimensional and the fluid is inviscid. In what follows, the case without blockage (i.e., $\alpha = 1$) is referred to as the intact pipe case.

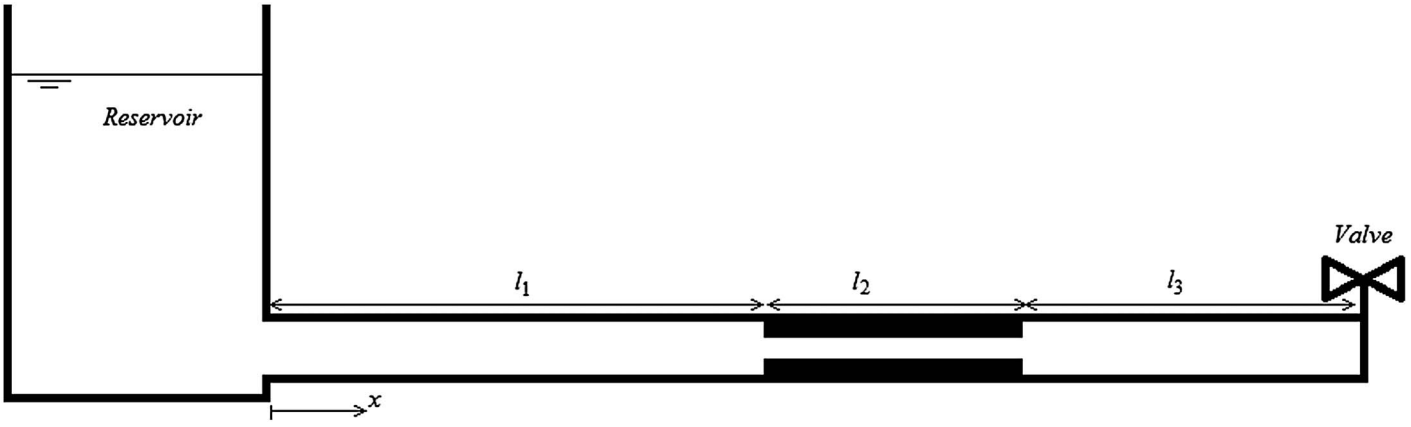

Fig. 1. Single blockage in a reservoir-pipe-valve system (bounded pipe system)

J. Hydraul. Eng., 2018, 144(1): 04017055

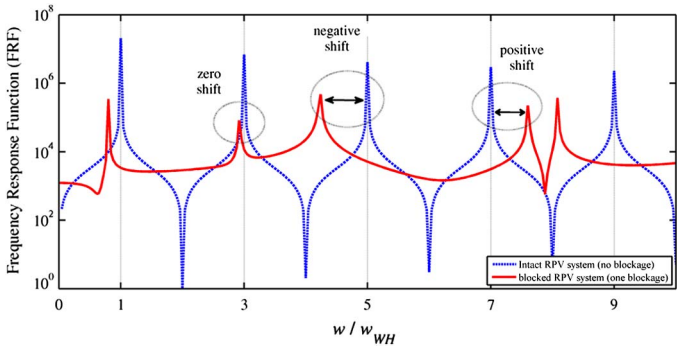

Fig. 2. Comparison between the FRFs of the intact and blocked RPV systems showing the eigenfrequency shifts at the first five resonant modes; $\eta_3 + \eta_2/2 = 0.562$, $\eta_2 = 0.15$, and $\alpha = 0.16$

The frequency response function (FRF) of the RPV system can be obtained by generating a transient signal at the valve, for example, by opening and/or closing the valve rapidly. Fig. 2 compares the FRF of the blocked RPV system (Fig. 1) and the FRF of the intact RPV system (i.e., with no blockage). A transient signal is generated by rapid valve closure with the closure time used in the numerical experiment equal to one time step (i.e., instantaneous closure). Fig. 2 shows the eigenfrequency shift due to the presence of the interior blockage in the pipe system. In Fig. 2, the wave modes are numbered along the abscissa. As observed in Fig. 2, the shift is almost zero at the second mode, whereas the eigenfrequencies of the blocked pipe system shift to the left at the third mode (a negative shift), and shift to the right at the fourth mode (a positive shift). The causes and mechanism for these observed eigenfrequency shifts is yet not discussed nor is it understood in the existing literature. This paper studies in detail the nature of the shift mechanism from an interior single blockage in a RPV system. The improved understanding of this shift phenomenon and the forward problem creates efficiencies in the computational solution of the corresponding inverse problem (i.e., blockage detection in pipe systems).

The dispersion relation governing eigenfrequencies of the blocked pipe system (Fig. 1) is given by El-Rahed and Wagner (1982) and Duan et al. (2011)

$$\alpha \cos(k_m l_1)\cos(k_m l_2)\cos(k_m l_3) - \cos(k_m l_1)\sin(k_m l_2)\sin(k_m l_3) - \alpha^2 \sin(k_m l_1)\sin(k_m l_2)\cos(k_m l_3) - \alpha \sin(k_m l_1)\cos(k_m l_2)\sin(k_m l_3) = 0 \quad (1)$$

which could also be written as

$$\cos(k_m L) + \frac{(1-\alpha)}{(1+\alpha)}\cos[k_m(l_1 - l_2 - l_3)] - \frac{(1-\alpha)}{(1+\alpha)}\cos[k_m(l_1 + l_2 - l_3)] - \frac{(1-\alpha)^2}{(1+\alpha)^2}\cos[k_m(l_1 - l_2 + l_3)] = 0 \quad (2)$$

where the subscript m = mth natural resonant mode; and $k_m = w_m/a$ is the mth wavenumber, with w_m being the mth eigenfrequency and a being the acoustic wave speed. When $\alpha = 1$, Eq. (2) becomes

$$\cos(k_m^0 L) = 0 \Rightarrow w_m^0 = a k_m^0 = 2\pi\left[(2m-1)\frac{a}{4L}\right]; \quad m = 1, 2, 3, \ldots \quad (3)$$

which is the dispersion relation of an intact pipe system with $k_m^0 = w_m^0/a$ being the mth wavenumber and w_m^0 being the mth eigenfrequency of the intact pipe system.

Figs. 3 and 4 show the eigenfrequency (w_m) variation with length $\eta_b = \eta_3 + 0.5\eta_2$ for the first five modes and different α values when $\eta_2 = 0.15$ and $\eta_2 = 0.027$, respectively. The cases for which $\alpha = 1$ in Figs. 3 and 4 represent the eigenfrequencies of the intact pipe case and are the straight horizontal lines. When $\alpha \neq 1$, the effect of the blockage is introduced and the eigenfrequency at a given mode m (w_m) deviates from the intact case (w_m^0) as shown in Figs. 3 and 4. The eigenfrequency shift is defined as $\Delta w_m = (w_m - w_m^0)$ and could take on positive, negative, or zero values (Figs. 3 and 4).

Comparing Figs. 3 and 4 shows that varying the blockage length induces a change in the maximum shift magnitude at given mode m and dimensionless area α. This feature is discussed in Louati et al. (2016), where it is shown that it is related to Bragg-type resonance (Mei 1985; Louati 2013). This resonance effect occurs when the reflection from the blockage is in phase with the incident wave, and leads to significant eigenfrequency shift. Bragg resonance conditions occur when the blockage length is of similar order of magnitude to wavelength [the exact conditions are given in Louati et al. (2016)]. At modes where a Bragg resonance condition occurs, the shift magnitude is high; otherwise, the shift magnitude is low. For short blockages, Bragg resonance occurs at shorter wavelengths (i.e., higher frequencies), and this accounts for the reduced shift magnitude at low modes in Fig. 4, for example, in the case of $\eta_2 = 0.027$.

Figs. 3 and 4 show that the magnitude of maximum positive shift and maximum negative shift vary for a given α at different modes m. Furthermore, for a given mode m, the location of the blockage where zero shift occurs varies with α. These features were not observed in the case of the blocked RPV system with blockage at the boundary (Louati and Ghidaoui 2016). This paper expands on the nature of, and reasons for, these observed features of eigenfrequency shift. This understanding is presently lacking in this field of research, yet it is precisely this insight that is essential to formulating useful dispersion relations [e.g., Eq. (2)] and developing viable models for identifying blockages in liquid pipelines.

For the case of shallow blockage, Louati and Ghidaoui (2016) derived an equation for the eigenfrequency shift based on the work done by the radiation pressure (Borgnis 1953; Beyer 1978; Louati and Ghidaoui 2016; Schroeder 1967), which is given by

$$\frac{\Delta w_m}{w_m^0} = \mathrm{Re}\left[\frac{-\xi_m}{h_m^{\mathrm{amp}}\overline{q_m^{\mathrm{amp}}}}\int_0^L \frac{d(h_m^0 \overline{q_m^0})}{dx}dx\right] \quad (4)$$

where $\xi_m = -i[(\rho g)/(2w_m^0 E_m^0)][(\Delta A)/A_0]h_m^{\mathrm{amp}}\overline{q_m^{\mathrm{amp}}}$; $h_m^0 = h_m^{\mathrm{amp}}\sin(k_m^0 x)$ and $q_m^0 = q_m^{\mathrm{amp}}\cos(k_m^0 x)$ are pressure head and flow harmonics for the intact pipe case, and h_m^{amp} and q_m^{amp} are their corresponding maximum amplitudes, respectively; $E_m^0 = (\rho A_0/2)[(g/a)^2(h_m^0)^2 + q_m^0/A_0^2]$ = energy of an intact pipe system; ρ = density; g = standard gravitational acceleration; $i = \sqrt{-1}$; $\Delta A = A - A_0$ with $A = A(x)$ being the cross-sectional area function; and Re = real part. Eq (4) is used for subsequent

J. Hydraul. Eng., 2018, 144(1): 04017055

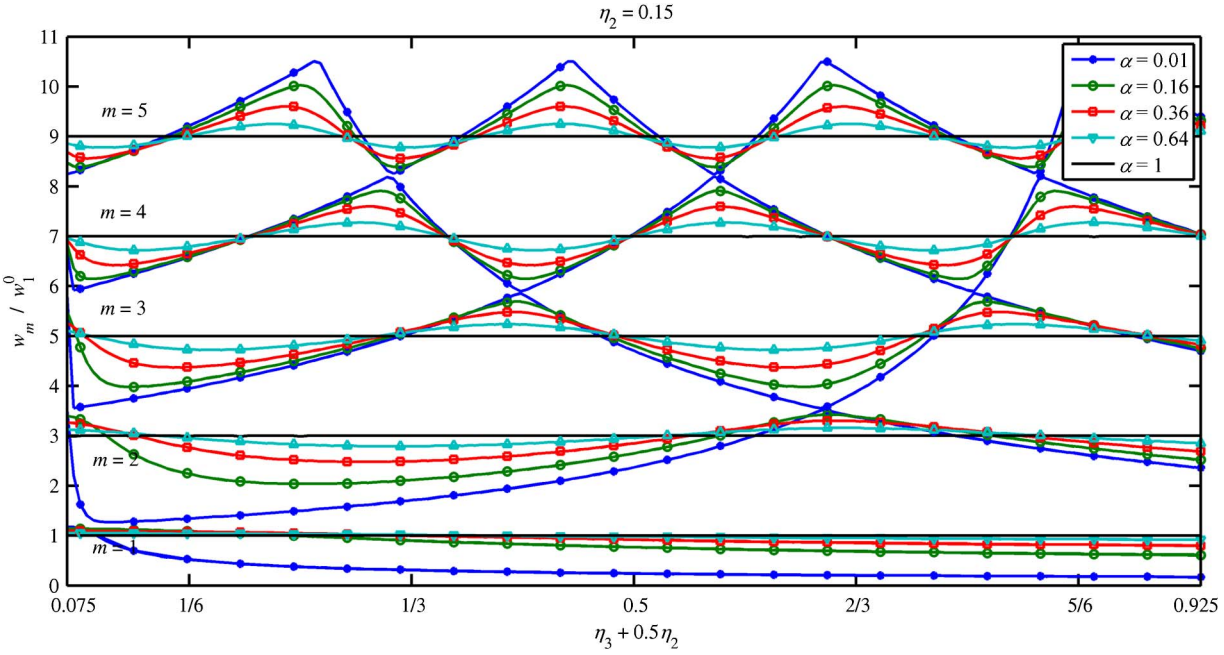

Fig. 3. Normalized eigenfrequency variation with length $\eta_b = \eta_3 + 0.5\eta_2$ of the first five modes for different α values when $\eta_2 = 0.15$

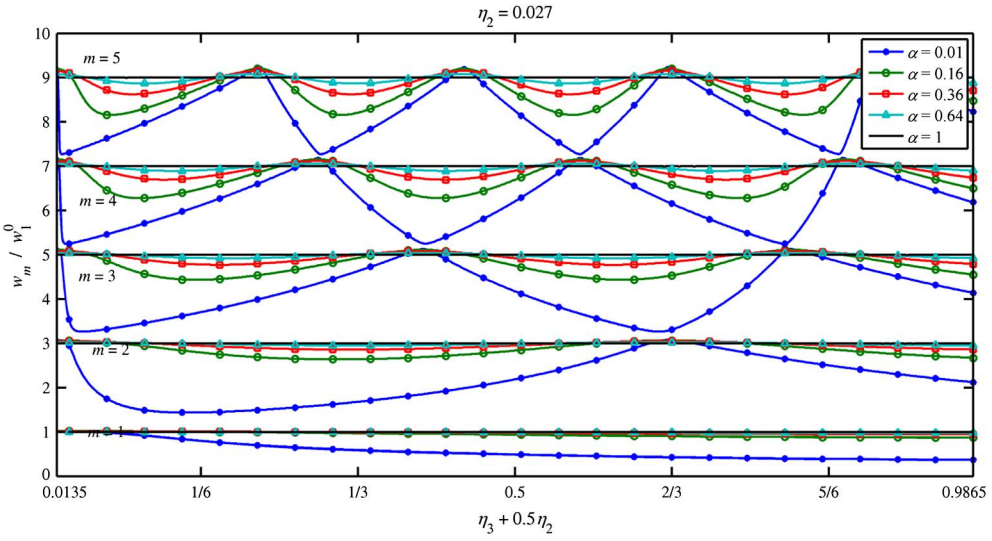

Fig. 4. Normalized eigenfrequency variation with length $\eta_b = \eta_3 + 0.5\eta_2$ of the first five modes for different α values when $\eta_2 = 0.027$

discussion and analysis of shift mechanism for the shallow blockage case.

Analysis and Discussion of Eigenfrequency Shift Variation for Interior Blockage with Small Radial Protrusion: Shallow Blockage Case

At a given mode m, Fig. 3 shows that the eigenfrequency-shift sign varies with the blockage location and mode number. Considering a blockage with small radial protrusion ($\alpha > 0.65$), the shift equation Eq. (4) is applied for the case of interior blockage and gives

$$\frac{\Delta w_m}{w_m^0} = \xi_m \left[\left(\frac{h_m^0 \overline{q_m^0}}{h_m^{\text{amp}} \overline{q_m^{\text{amp}}}} \right)_{l_1} - \left(\frac{h_m^0 \overline{q_m^0}}{h_m^{\text{amp}} \overline{q_m^{\text{amp}}}} \right)_{l_1+l_2} \right] \tag{5}$$

Inserting the pressure and flow harmonics into Eq. (5) gives

$$\frac{\Delta w_m}{w_1^0} = \frac{2}{\pi}(1-\alpha)\{\sin(k_m^0 l_1)\cos(k_m^0 l_1) - \sin[k_m^0(l_1+l_2)]\cos[k_m^0(l_1+l_2)]\} \tag{6}$$

$$\begin{aligned} \Rightarrow \frac{\Delta w_m}{w_1^0} &= \frac{(1-\alpha)}{\pi}\{\sin[(2m-1)\pi\eta_1] - \sin[(2m-1)\pi(\eta_1+\eta_2)]\} \\ &= \frac{(1-\alpha)}{\pi}\{\sin[(2m-1)\pi(\eta_3+\eta_2)] - \sin[(2m-1)\pi\eta_3]\} \\ &= \frac{(1-\alpha)}{\pi}\left\{2\sin\left[(2m-1)\frac{\pi}{2}\eta_2\right]\cos\left[(2m-1)\pi\left(\eta_3+\frac{\eta_2}{2}\right)\right]\right\} \end{aligned} \tag{7}$$

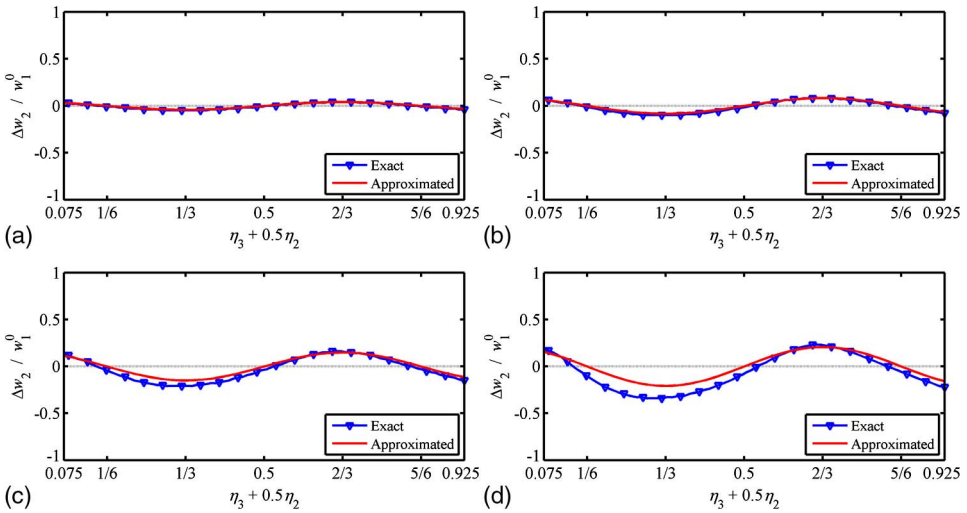

Fig. 5. Normalized eigenfrequency shift variation with length $\eta_3 + \eta_2/2$ for $m = 2$ and $\eta_2 = 0.15$: comparison between exact solution [Eq. (2)] and approximate solution [Eq. (7)]: (a) $\alpha = 0.9$; (b) $\alpha = 0.8$; (c) $\alpha = 0.64$; (d) $\alpha = 0.5$

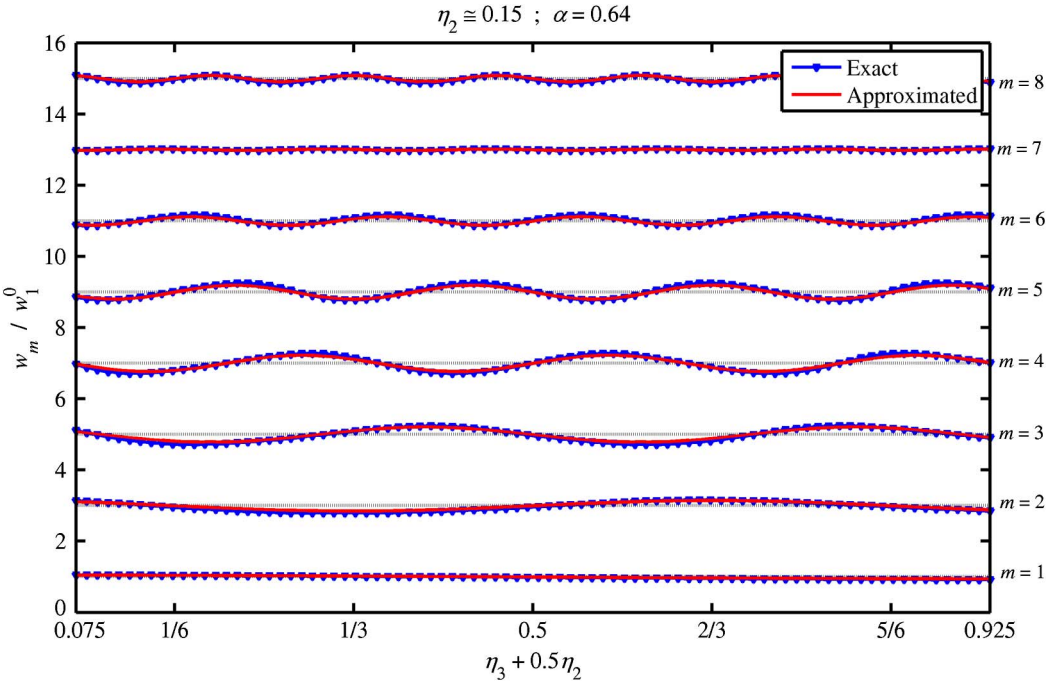

Fig. 6. Normalized eigenfrequency variation with length $\eta_3 + \eta_2/2$ for the first eight modes with $\alpha = 0.64$ and $\eta_2 = 0.15$: comparison between exact solution [Eq. (2)] and approximate solution [Eq. (7)]

Eq. (7) is identical to the simplified shift equation obtained in Duan et al. (2013), where they assumed a small shift and used Taylor expansion of the dispersion relation [Eq. (2)] around the intact pipe frequencies. Eq. (7) could also be obtained by using the energy approach in the form of the Ehrenfest theorem (Louati and Ghidaoui 2016; Fant 1975). Eq. (7) is found to compare well with experimental data (Duan et al. 2013). Fig. 5 gives the comparison between the approximated eigenfrequency shift from Eq. (7) and the exact eigenfrequency obtained using the dispersion relation [Eq. (2)] for different α values and shows good quantitative agreement between the exact shift solution from Eq. (2) and its approximate form [Eq. (7)] for $\alpha > 0.6$. Although not shown here, it is observed that there is overall qualitative agreement between the exact shift solution from Eq. (2) and its approximate form [Eq. (7)] for all α. A similar conclusion can be made for the other m modes as shown in Fig. 6, which gives the comparison between the exact and approximated eigenfrequency variation for the first eight modes with $\alpha = 0.64$. Such agreement supports the use of Eq. (7) to analyze the eigenfrequency shift signs and determine maximum shift locations.

Zero Eigenfrequency Shift

Setting Eq. (7) to zero gives the conditions for which the eigenfrequency shift is zero at a given mode m as follows:

J. Hydraul. Eng., 2018, 144(1): 04017055

$$\sin\left[(2m-1)\frac{\pi}{2}\eta_2\right]=0 \quad \text{or} \quad \cos\left[(2m-1)\pi\left(\eta_3+\frac{\eta_2}{2}\right)\right]=0 \tag{8}$$

which leads to

$$\eta_2=\frac{2(\bar{m}-1)}{(2m-1)} \quad \text{or} \quad \eta_3+\frac{\eta_2}{2}=\frac{2\bar{m}-1}{2(2m-1)};\quad \bar{m}=1,2,\ldots \tag{9}$$

The first equation in Eq. (9) corresponds to the Bragg resonance condition of total transmission (Louati et al. 2016; Louati 2016, 2013; Mei 1985) as follows:

$$\eta_2=\frac{2(\bar{m}-1)}{(2m-1)} \Leftrightarrow \frac{w_m^0}{w_{\bar{m}}^T(l_2)}=1 \Leftrightarrow l_2=\frac{(\bar{m}-1)}{2}\left[\frac{4L}{(2m-1)}\right] \tag{10}$$

where $w_{\bar{m}}^T$ = Bragg resonance frequency of total transmission (Louati 2016; Louati et al. 2016) for a single blockage in a pipe system. The condition in Eq. (10) states that the shift is zero if the blockage length is a multiple of the half-wavelength of the mth-mode harmonic. This condition is natural because if total wave transmission through the blockage occurs, then the blockage effect no longer exists, and therefore the system behaves as an intact pipe system.

The second equation in Eq. (9) corresponds to the location of the blockage midlength from the downstream boundary $(\eta_3+\eta_2/2)$, where

$$\sin\left[k_m^0 L\left(\eta_3+\frac{\eta_2}{2}\right)\right]=\pm\cos\left[k_m^0 L\left(\eta_3+\frac{\eta_2}{2}\right)\right] \Rightarrow \frac{h_m^0}{h_m^{\text{amp}}}=\pm\frac{q_m^0}{q_m^{\text{amp}}} \tag{11}$$

which states that the shift is zero if the blockage midlength is located at a position where the pressure head and the flow harmonics are equal in magnitude. At a given blockage length η_2, the first equation in Eq. (9) is independent of the blockage location, whereas the second equation depends on the blockage location. Either condition in Eq. (10) or Eq. (11) renders the right-hand side of Eq. (5) zero; thus, zero shift. Figs. 7(a and b) give the dimensionless pressure and flow harmonics variations along the pipe at modes $m=7$ and $m=2$, respectively. In this case, the blockage length is equal to half the wavelength of the seventh-mode harmonic, which is $\eta_2=2/(2\times7-1)=0.1538\approx0.15$. Three different locations are considered in Figs. 7(a and b). Fig. 7(a) shows that, at any blockage location along the pipe, the products of the pressure head and flow at the blockage boundaries are equal in magnitude and sign. Therefore, from Eq. (5), the shift is zero at any location along the pipe at Mode 7 as observed in Fig. 6. In Fig. 7(b), the first equation in Eq. (9) is not satisfied where the blockage length is smaller than half the wavelength of the second-mode harmonic. The blockage location cases shown in Fig. 7(b) satisfy the second equation in Eq. (9) where the blockage midlength is situated at the position of equal pressure head and flow magnitudes. At these specific blockage locations, the products of the pressure head and flow at the blockage boundaries are also equal, which leads to zero shift. Consequently, the second equation in Eq. (9) gives the zero shift location at any given mode m as observed in Figs. 3 and 6 except when the blockage length is a multiple of the half-wavelength of the mth-mode harmonic where the shift becomes zero at any blockage location along the pipe.

Positive and Negative Eigenfrequency Shift

As observed from Figs. 3 and 6, the shift sign alternates between consecutive zero shift locations. Moreover, within two zero shift locations, the shift reaches either a positive or negative maximum shift. This section studies the mechanism causing this variation of shift sign and magnitude for shallow blockage case. Conditions for

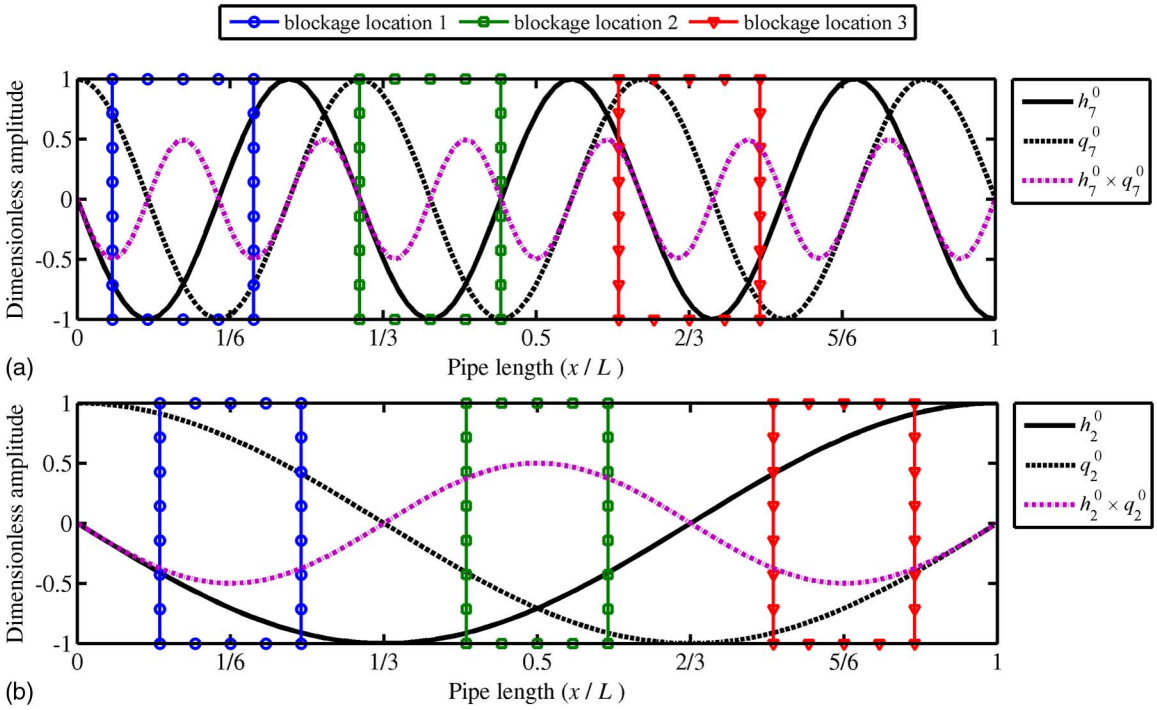

Fig. 7. Dimensionless pressure head and flow harmonics variation along the pipe where different blockage location cases are shown to discuss the zero shift equations [Eq. (9)]: (a) seventh mode of pressure and flow harmonics; (b) second mode of pressure and flow harmonics

J. Hydraul. Eng., 2018, 144(1): 04017055

maximum shift are obtained by equating the gradient of Eq. (7) to zero, which gives

$$\cos\left[(2m-1)\frac{\pi}{2}\eta_2\right]=0 \quad \text{and} \quad \sin\left[(2m-1)\pi\left(\eta_3+\frac{\eta_2}{2}\right)\right]=0 \tag{12}$$

yielding

$$\eta_2=\frac{2\bar{m}-1}{(2m-1)};\quad \bar{m}=1,2,\ldots$$

and

$$\eta_3+\frac{\eta_2}{2}=\frac{\overline{m'}}{2m-1};\quad \overline{m'}=1,2,\ldots \tag{13}$$

The first equation in Eq. (13) corresponds to the Bragg resonance condition of maximum reflection (Louati et al. 2016; Louati 2016, 2013; Mei 1985) as follows:

$$\eta_2=\frac{2\bar{m}-1}{2m-1}\Leftrightarrow\frac{w_m^0}{w_{\bar{m}}^R(l_2)}=1\Leftrightarrow l_2=\frac{(2\bar{m}-1)}{4}\left(\frac{4L}{2m-1}\right) \tag{14}$$

where $w_{\bar{m}}^R$ = Bragg resonance frequency of total reflection (Louati 2016; Louati et al. 2016) for a single blockage in a pipe system. The condition in Eq. (14) states that the shift is maximum if the blockage length is an odd multiple of the quarter-wavelength of the mth-mode harmonic. Waves propagating at Bragg resonance frequency of maximum reflection interact most with, and therefore it is natural that they induce, the largest eigenfrequency shift.

The second equation in Eq. (13) corresponds to the location of the blockage midlength from the downstream boundary $(\eta_3+\eta_2/2)$ where

$$\begin{matrix}\eta_3+\frac{\eta_2}{2}=\frac{2\overline{m'}}{2m-1}\\ \text{or}\\ \eta_3+\frac{\eta_2}{2}=\frac{2\overline{m'}-1}{2m-1}\end{matrix}\Rightarrow\begin{cases}\sin\left[k_m^0L\left(\eta_3+\frac{\eta_2}{2}\right)\right]=0\\ \text{or}\\ \cos\left[k_m^0L\left(\eta_3+\frac{\eta_2}{2}\right)\right]=0\end{cases}\Rightarrow\begin{cases}\frac{h_m^0}{h_m^{\text{amp}}}=0\\ \text{or}\\ \frac{q_m^0}{q_m^{\text{amp}}}=0\end{cases} \tag{15}$$

which states that the shift is maximum if the blockage midlength is located at either a pressure node or a stagnation point. Conversely to the zero shift case, where either satisfied condition in Eq. (9) leads to a zero shift, the maximum shift requires both equations in Eq. (13) to be fulfilled. That is, the maximum shift is given when the blockage length is an odd multiple of the quarter-wavelength of the mth-mode harmonic and its midlength is located at a position of either a pressure node or stagnation point. Fig. 8 gives the dimensionless pressure and flow harmonics variations along the pipe at modes $m=4$. In this case, the blockage length is equal to the quarter-wavelength of the fourth-mode harmonic, which is $\eta_2=1/(2\times4-1)\approx0.15$. Three different locations are considered in Fig. 8 to discuss the properties of Eq. (13). Blockage Locations 1 and 3 are such that the blockage midlength is placed respectively at a stagnation point and pressure node where both equations in Eq. (13) are satisfied. In these cases, Fig. 8 shows that the products of the pressure head and flow at the blockage boundaries are equal in magnitude but with different signs. Therefore, the work done at the boundaries in Eq. (5) are added up, and because the product of sine and cosine is maximum when these two functions are equal, Eq. (5) gives the maximum shift magnitude. At Blockage Locations 1 and 3, Fig. 6 shows that the shift magnitude is maximum.

Blockage Location 2 in Fig. 8 is such that the blockage midlength is placed at a location of equal pressure head and flow, which satisfies the second condition of zero shift [Eq. (9)] but not the second equation in Eq. (13). In this case, the product of the pressure head and flow at the blockage boundaries becomes of equal magnitude and sign. Therefore, from Eq. (5), the shift is zero as observed from Fig. 6. This shows the necessity of satisfying both conditions in Eq. (13) to produce maximum shift.

To distinguish between positive and negative maximum shifts, the determinant of the Hessian matrix ($\mathbf{D}_H$) is computed and analyzed (see the Appendix). At the critical points conditions [Eq. (12)], one obtains

$$\mathbf{D}_H=\left[\frac{(1-\alpha)}{\pi}\right]^2[(2m-1)\pi]^4(-1)^{2(\bar{m}+\overline{m'}+1)}>0 \tag{16}$$

Therefore, if $\bar{m}$ and $\overline{m'}$ have the same parity, then the maximum shift is negative. However, if $\bar{m}$ and $\overline{m'}$ have different parity, then the maximum shift is positive. This means that at a given Bragg resonance mode ($\bar{m}$) of maximum reflection [see first condition in Eq. (13)], if $\bar{m}$ is even, then the maximum shift is either positive or negative depending on whether the blockage midlength is located respectively at a pressure node or stagnation point [Eq. (15)], and vice versa if $\bar{m}$ is odd.

For example, Fig. 8 shows the pressure and flow harmonics at mode $m=4$, which corresponds to the first Bragg resonance frequency of maximum reflection ($\bar{m}=1$). The midlength of Blockage Location 1 in Fig. 8 is at a stagnation point, which from Fig. 6 gives a positive maximum shift as expected. On the other

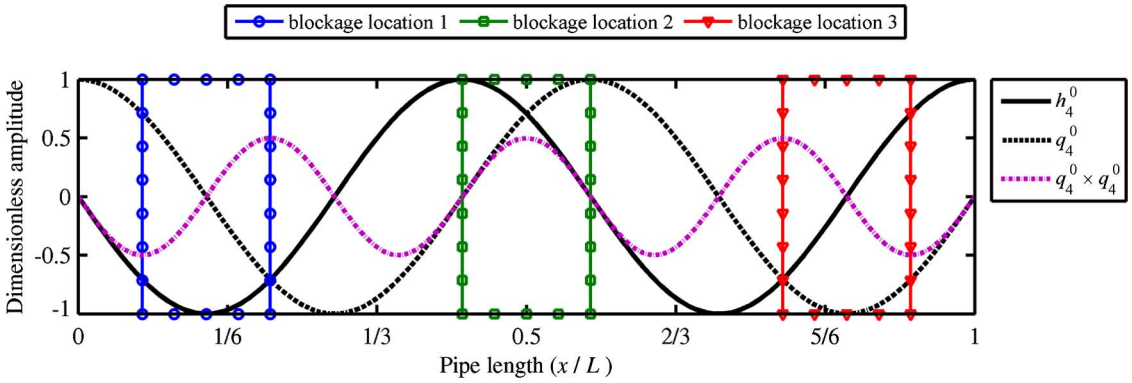

Fig. 8. Dimensionless pressure head and flow harmonics of the fourth mode where different blockage location cases are shown to discuss the maximum shift equations [Eq. (13)]

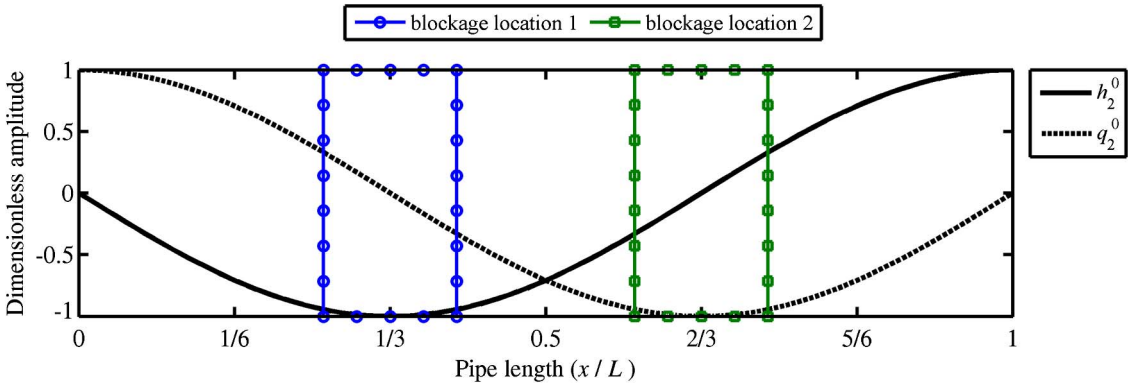

Fig. 9. Dimensionless pressure head and flow harmonics of the second mode where different blockage location cases are shown to discuss the maximum shift equations at given mode m [Eqs. (17) and (19)]

hand, the midlength of Blockage Location 3 in Fig. 8 is at a pressure node, which from Fig. 6 gives a negative maximum shift, also as expected.

Eq. (13) gives the conditions for absolute maximum shift, which is given at specific modes that satisfy the Bragg resonance condition of maximum reflection. However, at any given mode m, the eigenfrequency variation undergoes local maximum shift, although the Bragg resonance condition of maximum reflection is not satisfied. The location of those local maximum shifts at any given mode m can be determined for a fixed blockage length η_2. Therefore, assuming a fixed blockage length η_2 and equating to zero the first derivative of the shift equation [Eq. (7)] with respect to the midlength blockage location $(\eta_3 + \eta_2/2)$ gives

$$\sin\left[(2m-1)\pi\left(\eta_3+\frac{\eta_2}{2}\right)\right]=0 \Rightarrow \eta_3+\frac{\eta_2}{2}=\frac{\bar{m}}{2m-1} \tag{17}$$

which is the second condition in Eq. (13). The maximum shift sign is obtained by computing the second derivative at the maximum shift locations as follows:

$$\frac{\partial^2(\overline{\Delta w_m}/w_1^0)}{\partial(\eta_3+\eta_2/2)^2}=2\frac{(1-\alpha)}{\pi}[(2m-1)\pi]^2\sin\left[(2m-1)\frac{\pi}{2}\eta_2\right](-1)^{\bar{m}+1} \tag{18}$$

Knowing that $\sin[(2m-1)\pi\eta_2/2]$ changes sign between two consecutive Bragg resonance frequencies of total transmission [Eq. (10)], Eq. (18) gives

$$\operatorname{sgn}\left[\frac{\partial^2(\overline{\Delta w_m}/w_1^0)}{\partial(\eta_3+\eta_2/2)^2}\right] = (-1)^{n_T+\bar{m}}\begin{cases}\text{if } > 0 \Rightarrow \text{maximum shift is negative}\\ \text{if } < 0 \Rightarrow \text{maximum shift is positive}\end{cases} \tag{19}$$

where sgn = signum function; and n_T = integer that gives the number of modes region between two consecutive Bragg resonance frequencies of total transmission defined as

$$n_T=\text{Floor}\left[(2m-1)\frac{\eta_2}{2}\right]+1 \tag{20}$$

where Floor = function that gives the largest previous integer. The second derivative in Eq. (19) is positive when n_T and $\bar{m}$ have the same parity, which leads to negative maximum shift, and positive when n_T and $\bar{m}$ have different parity, which leads to positive maximum shift. This means that at a given m such that n_T is even, the maximum shift is positive or negative when the blockage midlength is located respectively at a pressure node or stagnation point [Eq. (15)], and vice versa if n_T is odd. For example, Fig. 9 gives the dimensionless pressure and flow harmonics at mode $m = 2$, where the blockage length is $\eta_2 \approx 0.15$, which gives $n_T = 1$ [Eq. (20)]. Two blockage location cases are shown in Fig. 9. The midlength of Blockage Locations 1 and 2 are placed, respectively, at a stagnation point and a pressure node. Fig. 6 shows that at these blockage locations the maximum shift is respectively positive and negative, a result that is expected from Eq. (19).

Analysis and Discussion of Eigenfrequency Shift Variation for Interior with Moderate and Large Radial Protrusion

Variation of Zero Shift Locations with the Radial Protrusion of the Blockage

For the case of blocked pipe system with blockage at the boundary (Louati and Ghidaoui 2016), the zero shift locations are independent of α. However, for the interior blockage case, Figs. 3 and 4 show that the zero shift locations at a given mode vary with α except at modes corresponding to the Bragg resonance frequency of maximum reflections (e.g., see fourth mode in Fig. 3). In fact, at these Bragg resonance modes, the pipe system with interior blockage behaves as if the blockage is located at the boundary (Louati et al. 2016). To determine the variation of the zero shift locations at modes other than the Bragg resonance modes, the dispersion relation for blocked RPV system with interior blockage [Eq. (2)] is rewritten as follows:

$$\begin{aligned}&\cos(k_mL)+\frac{(1-\alpha)}{(1+\alpha)}\cos\{k_mL[1-(2\eta_3+\eta_2)-\eta_2]\}\\&-\frac{(1-\alpha)}{(1+\alpha)}\cos\{k_mL[1-(2\eta_3+\eta_2)+\eta_2]\}\\&-\frac{(1-\alpha)^2}{(1+\alpha)^2}\cos[k_mL(1-2\eta_2)]=0\end{aligned} \tag{21}$$

Using the fact that at zero shift, $k_m = k_m^0 = (2m-1)[\pi/(2L)]$ gives

$$\sin\left[(2m-1)\frac{\pi}{2}(2\eta_3+\eta_2)+(2m-1)\frac{\pi}{2}\eta_2\right] - \sin\left[(2m-1)\frac{\pi}{2}(2\eta_3+\eta_2)-(2m-1)\frac{\pi}{2}\eta_2\right] - \frac{(1-\alpha)}{(1+\alpha)}\sin\left[(2m-1)\frac{\pi}{2}2\eta_2\right]=0 \quad (22)$$

Using trigonometric manipulation on Eq. (22) yields

$$2\sin\left[(2m-1)\frac{\pi}{2}\eta_2\right]\cos\left[(2m-1)\frac{\pi}{2}(2\eta_3+\eta_2)\right] - 2\frac{(1-\alpha)}{(1+\alpha)}\sin\left[(2m-1)\frac{\pi}{2}\eta_2\right]\cos\left[(2m-1)\frac{\pi}{2}\eta_2\right]=0 \quad (23)$$

which gives

$$\left\{\cos\left[(2m-1)\frac{\pi}{2}(2\eta_3+\eta_2)\right] - \frac{(1-\alpha)}{(1+\alpha)}\cos\left[(2m-1)\frac{\pi}{2}\eta_2\right]\right\}\sin\left[(2m-1)\frac{\pi}{2}\eta_2\right]=0 \quad (24)$$

There are two possible solutions for Eq. (24). The first is

$$\sin[(2m-1)\pi\eta_2/2]=0 \quad (25)$$

which gives the Bragg resonance frequencies of total transmission and corresponds to the first equation in Eq. (9) for the small radial protrusion case. The second is given by

$$\cos\left[(2m-1)\frac{\pi}{2}(2\eta_3+\eta_2)\right]-\frac{(1-\alpha)}{(1+\alpha)}\cos\left[(2m-1)\frac{\pi}{2}\eta_2\right]=0 \quad (26)$$

which has the following solution

$$(2m-1)\frac{\pi}{2}(2\eta_3+\eta_2) = -\arccos\left\{(-1)^{\bar{m}}\frac{(1-\alpha)}{(1+\alpha)}\cos\left[(2m-1)\frac{\pi}{2}\eta_2\right]\right\}+\bar{m}\pi \quad (27)$$

leading to

$$\eta_3+\frac{\eta_2}{2}=\frac{2\bar{m}-\frac{2}{\pi}\arccos\left\{(-1)^{\bar{m}}\frac{(1-\alpha)}{(1+\alpha)}\cos[(2m-1)\frac{\pi}{2}\eta_2]\right\}}{2(2m-1)} \quad (28)$$

Eq. (28) gives the zero shift locations ($\bar{m}$) at a given mode m and for a given dimensionless area α. For example, the zero shift locations from Eq. (28) at the second mode ($m=2$) and for $\alpha=0.16$ and $\eta_2=0.15$ are

$$\eta_3+\frac{\eta_2}{2}=0.1048; \qquad \eta_3+\frac{\eta_2}{2}=0.5619; \qquad \eta_3+\frac{\eta_2}{2}=0.7715 \quad (29)$$

which agrees with the zero shift locations observed in Fig. 3.

Notice that when

$$\cos[(2m-1)\pi\eta_2/2]=0 \quad (30)$$

which gives the Bragg resonance frequencies of maximum reflection, Eq. (28) becomes

$$\eta_3+\frac{\eta_2}{2}=\frac{2\bar{m}-1}{2(2m-1)} \quad (31)$$

which is independent of α and corresponds to the second zero shift equation in Eq. (9) for small radial protrusion case. Moreover, Eq. (30) gives

$$\eta_2=\frac{2\overline{m'}-1}{(2m-1)}; \quad \overline{m'}=1,2,3,\ldots,<m \quad (32)$$

and when inserted into Eq. (31) yields

$$\eta_3=\frac{\overline{m''}}{(2m-1)}; \qquad \overline{m''}\equiv\bar{m}-\overline{m'}-1=1,2,3,\ldots \quad (33)$$

which could be written as

$$\frac{l_3}{(l_1+l_3)}(1-\eta_2)=\frac{\overline{m''}}{(2m-1)}\Rightarrow\frac{l_3}{(l_1+l_3)}=\frac{\overline{m''}}{2(m-\overline{m'})} \quad (34)$$

Eq. (34) can be shown to correspond to the zero shift locations for the case of a blocked reservoir-pipe-reservoir (RPR) system with blockage at the boundary. This is because at Bragg resonance frequencies of maximum reflections, the blocked RPV system with interior blockage behaves as blocked RPR system with total length l_1+l_3 and having a blockage at the downstream boundary with length l_3 (Louati et al. 2016).

Eq. (28) could be written as follows:

$$\eta_3+\frac{\eta_2}{2}=\frac{2\bar{m}-1}{2(2m-1)}+\frac{1-\frac{2}{\pi}\arccos\{(-1)^{\bar{m}}\frac{1-\alpha}{1+\alpha}\cos[(2m-1)\frac{\pi}{2}\eta_2]\}}{2(2m-1)} \quad (35)$$

The first term on the right-hand side of Eq. (35) is the zero shift locations for the case of blockage with small radial protrusion (shallow blockage). The second term on the right-hand side represents the deviation from the zero shift locations of shallow blockage case. The deviations range from

$$\left[\frac{-1}{2(2m-1)} \text{ to } \frac{1}{2(2m-1)}\right] \quad (36)$$

These deviations become very small at high modes. For example, at modes $m=2$ and $m=3$, the deviation range becomes

$$\left[\frac{-1}{6} \text{ to } \frac{1}{6}\right] \quad \text{and} \quad \left[\frac{-1}{10} \text{ to } \frac{1}{10}\right] \quad (37)$$

respectively. Therefore Eq. (35) could be approximated by the equation of zero shift locations for shallow blockages [Eq. (31)] at relatively high modes.

Variation of the Maximum Shift Locations and Magnitudes

In both interior blockage and blockage at the boundary cases, the maximum shift locations change as the radial protrusion of the blockage (α) varies (Figs. 3 and 4). For the case of blockage at the boundary, the maximum shift locations could be determined from Louati and Ghidaoui (2016). To obtain the maximum shift locations for the case of interior blockage, the dispersion relation [Eq. (2)] is rewritten as follows:

$$\cos(k_mL)+\frac{1-\alpha}{1+\alpha}(\cos\{k_mL[1-(2\eta_3+\eta_2)-\eta_2]\}-\cos\{k_mL[1-(2\eta_3+\eta_2)+\eta_2]\})-\left(\frac{1-\alpha}{1+\alpha}\right)^2\cos[k_mL(1-2\eta_2)]=0 \tag{38}$$

which gives

$$\cos(k_mL)+\frac{1-\alpha}{1+\alpha}(2\sin\{k_mL[1-(2\eta_3+\eta_2)]\}\sin(k_mL\eta_2)-\frac{1-\alpha}{1+\alpha}\cos[k_mL(1-2\eta_2)])=0 \tag{39}$$

The second term in Eq. (39) represents the effect of the blockage on the dispersion relation. In fact, for $\alpha=1$, this second term vanishes and Eq. (39) becomes identical to the dispersion relation of an intact RPV system [Eq. (3)]. Therefore, the shift is maximum when the term inside the curly brackets is maximum. Denoting this term by

$$\Theta=2\sin\{k_mL[1-(2\eta_3+\eta_2)]\}\sin(k_mL\eta_2)-\frac{1-\alpha}{1+\alpha}\cos[k_mL(1-2\eta_2)] \tag{40}$$

and equating its gradient to zero gives

$$\frac{\partial\Theta}{\partial(k_mL)}=\left\{2([1-(2\eta_3+\eta_2)]\cos\{k_m^{\max}L[1-(2\eta_3+\eta_2)]\}\times\sin(k_m^{\max}L\eta_2)+\eta_2\sin\{k_m^{\max}L[1-(2\eta_3+\eta_2)]\}\times\cos(k_m^{\max}L\eta_2))+\frac{1-\alpha}{1+\alpha}(1-2\eta_2)\times\sin[k_m^{\max}L(1-2\eta_2)]\right\}=0$$

and

$$\frac{\partial\Theta}{\partial(2\eta_3+\eta_2)}=-2k_m^{\max}L\cos\{k_m^{\max}L[1-(2\eta_3+\eta_2)]\}\times\sin(k_m^{\max}L\eta_2)=0 \tag{41}$$

which yields

$$2(-1)^{\bar{m}+1}\eta_2\cos(k_m^{\max}L\eta_2)+\frac{1-\alpha}{1+\alpha}(1-2\eta_2)\sin[k_m^{\max}L(1-2\eta_2)]=0$$

and

$$\cos\{k_m^{\max}L[1-(2\eta_3+\eta_2)]\}=0\Rightarrow k_m^{\max}L[1-(2\eta_3+\eta_2)]=(2\bar{m}-1)\frac{\pi}{2} \tag{42}$$

Solving for the second equation in Eq. (42) gives the blockage locations at maximum eigenfrequencies as follows:

$$\eta_3+\frac{\eta_2}{2}=\frac{1}{2}\left[1-\frac{2(m-\bar{m})-1}{w_m^{\max}/w_1^0}\right];\quad \text{with}\quad\begin{cases}\dfrac{\eta_2}{2}<\eta_3+\dfrac{\eta_2}{2}<1-\dfrac{\eta_2}{2}\\ \bar{m}=1,2,3,\ldots\end{cases} \tag{43}$$

By studying the sign of the Hessian matrix determinant, it can be shown that the distinction between maximum and minimum eigenfrequency magnitudes is governed by Eq. (19). To verify Eq. (43), consider the case of $\eta_2=0.15$ in Fig. 3 where the maximum and minimum eigenfrequency magnitudes at mode $m=3$ and $\alpha=0.16$ are $w_3^{\max}/w_1^0=5.69$ and $w_3^{\min}/w_1^0=4$, respectively. Inserting the maximum eigenfrequency magnitude into Eq. (43) and taking into account Eq. (19) gives

$$\eta_3+\frac{\eta_2}{2}=0.4121\quad\text{or}\quad\eta_3+\frac{\eta_2}{2}=0.7636 \tag{44}$$

which agrees with the maximum positive shift locations observed in Fig. 3. Inserting the maximum eigenfrequency magnitude into Eq. (43) and taking into account Eq. (19) gives

$$\eta_3+\frac{\eta_2}{2}=0.125\quad\text{or}\quad\eta_3+\frac{\eta_2}{2}=0.625 \tag{45}$$

which also agrees with the maximum negative shift locations observed in Fig. 3.

For the cases of blockage with small radial protrusion, the positive and negative shift magnitudes are about the same at a given mode [Fig. 6 and Eq. (7)]. However, Figs. 3 and 4 show that the magnitudes of the positive and negative maximum shifts oscillate as the mode number increases. For example, Fig. 3 shows that at the second and third modes, the magnitude of the positive maximum shift is lower than the negative maximum shift. However, at the fourth mode, which is near the Bragg resonance condition of maximum reflection, both negative and positive maximum shift magnitudes are the same. At the fifth and sixth modes, the magnitude of the positive maximum shift becomes larger than the negative shift. Figs. 10 and 11 give the eigenfrequency (w_m) variation with length $\eta_b=\eta_3+0.5\eta_2$ for the first 15 and 40 modes for $\eta_2=0.15$ and $\eta_2=0.027$, respectively. Overall, Figs. 10 and 11 show that between two modes where maximum transmission occurs, the magnitude of the positive maximum shift is low at low modes and increases as the frequency increases, and conversely, the negative maximum shift is high at low modes and decreases as the frequency increases. Both negative and positive shift magnitudes become the same at the Brag resonance frequency of maximum reflection.

The solution of the first equation in Eq. (42) gives the maximum eigenfrequency magnitudes at a given mode m. However, to date, attempts to solve for the first equation in Eq. (42) and find a closed form for the maximum eigenfrequency at a given mode m have failed. Fortunately, the features observed for the maximum shift variation can be explained qualitatively. Eqs. (35) and (36) show that the variation range of zero shift location is

$$\eta_3+\frac{\eta_2}{2}=\left[\frac{\bar{m}-1}{(2m-1)}\ \text{to}\ \frac{\bar{m}}{(2m-1)}\right] \tag{46}$$

The boundaries in Eq. (46) are the locations of a positive and negative shift for shallow blockages. This implies that the zero shift locations could coincide with a maximum shift location, preventing the maximum shift from occurring. To further illustrate this effect, consider the case of a blockage with large radial protrusion such that $\alpha\approx 0$. In this case, the zero shift equation in Eq. (28) gives

$$\eta_3+\frac{\eta_2}{2}=\frac{2\bar{m}-\frac{2}{\pi}\arccos\{(-1)^{\bar{m}}\cos[(2m-1)\frac{\pi}{2}\eta_2]\}}{2(2m-1)} \tag{47}$$

which leads to two cases, depending on whether the zero shift location $\bar{m}$ is even or odd as follows:

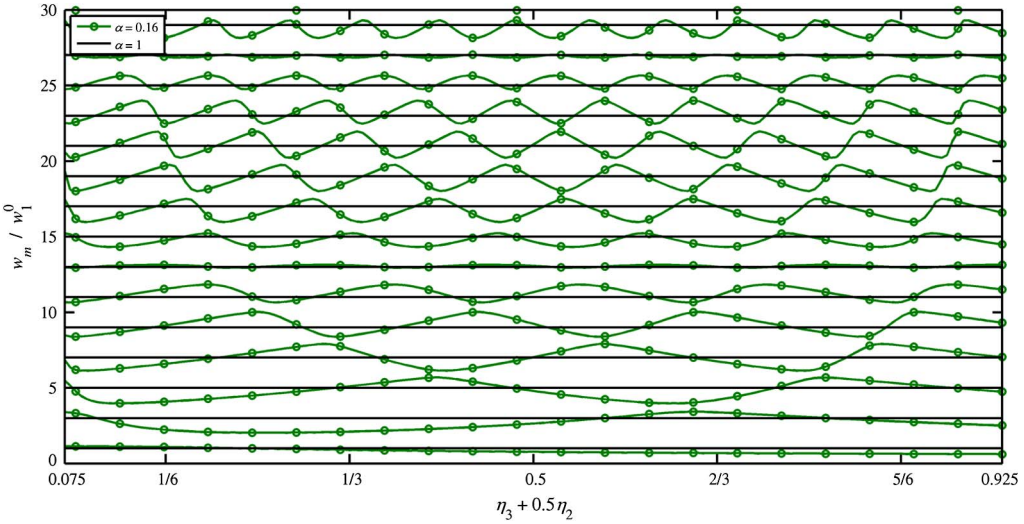

Fig. 10. Normalized eigenfrequency variation with length $\eta_b = \eta_3 + 0.5\eta_2$ of the first 15 modes when $\alpha = 0.16$ and $\eta_2 = 0.15$; data similar to data found in Louati et al. (2016) was used to calculate the results

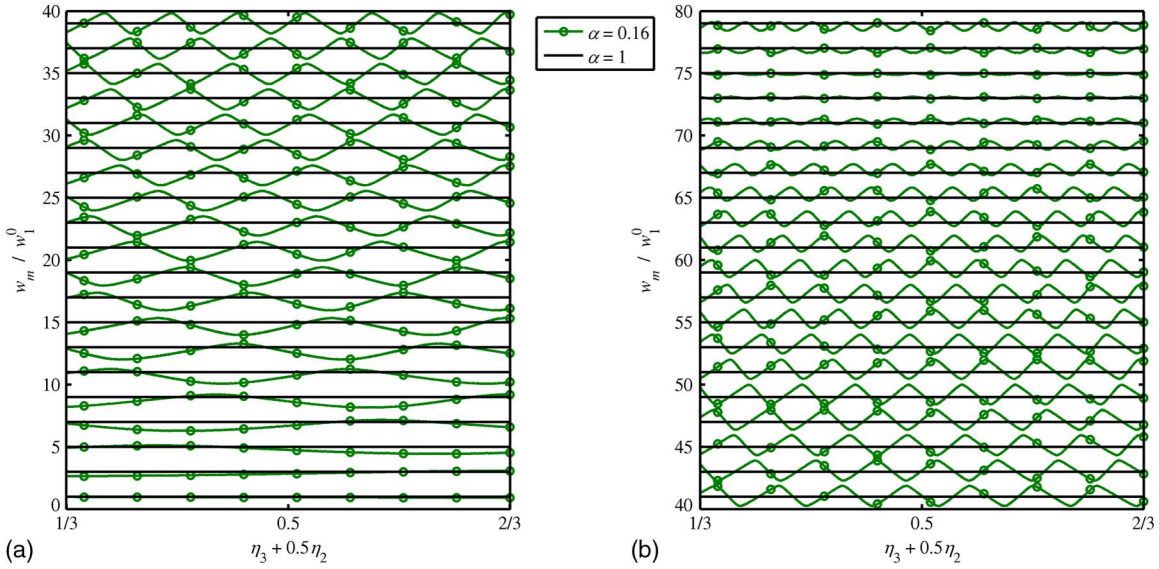

Fig. 11. Normalized eigenfrequency variation with length $\eta_b = \eta_3 + 0.5\eta_2$ when $\alpha = 0.16$ and $\eta_2 = 0.027$: (a) the first 20 modes; (b) modes $m = 21$ to $m = 40$; data similar to data found in Louati et al. (2016) was used to calculate the results

$$\eta_3 + \frac{\eta_2}{2} = \frac{\bar{m} - 1}{(2m - 1)} + \frac{\eta_2}{2} \quad \text{if } \bar{m} \text{ is odd}$$
$$\eta_3 + \frac{\eta_2}{2} = \frac{\bar{m}}{(2m - 1)} - \frac{\eta_2}{2} \quad \text{if } \bar{m} \text{ is even} \tag{48}$$

In a more general, and simpler, form, Eq. (48) becomes

$$\eta_3 + \frac{\eta_2}{2} = \frac{2\bar{m}}{(2m - 1)} \pm \frac{\eta_2}{2} \tag{49}$$

This shows that the zero shift location for severe blockages could approach the maximum shift at even locations for certain modes. Knowing that the maximum shift sign at even locations changes at different modes, the zero shift locations approach positive maximum shift locations at certain modes, and approach the negative maximum shift locations at other modes. For example, Figs. 3 and 10 show that for the case of $\eta_2 = 0.15$, the second maximum shift (as $\eta_3 + \eta_2/2$ increases) is positive at modes $m = 2$ and $m = 3$. Figs. 3 and 10 show that at those modes, the zero shift locations are close to the maximum positive shift location, and therefore the magnitude of the positive shift is reduced.

Moreover, for very short blockages, Eq. (48) shows that two consecutive zero shifts take almost the same location at low modes. Because a shift occurs between two zero shift locations, this would prevent the shift at even locations from taking place. For example, the case of $\eta_2 = 0.027$ in Figs. 4 and 11 shows that at low modes such as $m = 2$, almost only negative shifts occur and that the zero shift locations coincide at almost $\eta_3 + \eta_2/2 = 2/3$.

Eq. (49) approaches the zero shift locations for small radial protrusion when

$$\eta_3 + \frac{\eta_2}{2} = \frac{2m''}{(2m - 1)} \pm \frac{\eta_2}{2} \approx \frac{2m' - 1}{2(2m - 1)}$$
$$\Rightarrow \mp\eta_2 \approx \frac{2(2m'' - m') + 1}{(2m - 1)} \tag{50}$$

which is the condition for Bragg resonance frequency of maximum reflections [Eq. (14)]. This is as shown in Eq. (31), and as expected from Figs. 10 and 11. On the other hand, Eq. (49) approaches the odd maximum shift locations when

$$\eta_3 + \frac{\eta_2}{2} = \frac{2\bar{m}}{(2m-1)} \pm \frac{\eta_2}{2} \approx \frac{2\overline{m'}-1}{(2m-1)}$$
$$\Rightarrow \mp\eta_2 \approx \frac{2(2\bar{m}-2\overline{m'}+1)}{(2m-1)} \tag{51}$$

which is the condition for Bragg resonance frequency of total transmission [Eq. (10)]. In addition, Eqs. (19) and (20) show that the maximum negative shifts occur at odd locations for modes below the first Bragg resonance frequency of total transmission. This is why Figs. 10 and 11 show that as the mode number approaches the Bragg resonance frequency of total transmission, the magnitude of negative shifts decreases and the zero shift locations move toward the negative shift locations. Once the mode number exceeds the Bragg resonance frequency of total transmission, the zero shift locations switch from being close to the negative shift locations to being near the positive shift locations. This is because, from Eqs. (19) and (20), the positive shift switches from being at even locations to odd locations when the mode number crosses a Bragg resonance frequency of total transmission.

Low-Frequency Approximation

For a severe blockage case, Fig. 3 shows that the lowest mode takes mostly negative shift. In this case, if the first eigenfrequency is assumed to be very small ($w_1/w_1^0 \ll 1$), then a first-order Taylor expansion could be applied to sine and cosine functions in the dispersion relation [Eq. (2)], which gives

$$\alpha - (k_1L)^2\eta_2\eta_3 - \alpha^2(k_1L)^2\eta_1\eta_2 - \alpha(k_1L)^2\eta_1\eta_3 \approx 0$$
$$\Rightarrow \frac{w_1}{w_1^0} \approx \frac{2}{\pi}\sqrt{\frac{\alpha}{\alpha^2\eta_1\eta_2 + \alpha\eta_1\eta_3 + \eta_2\eta_3}} \tag{52}$$

Considering that $\alpha \ll 1$, Eq. (52) becomes

$$\frac{w_1}{w_1^0} \approx \frac{2}{\pi}\sqrt{\frac{\alpha}{\eta_2\eta_3}} \tag{53}$$

To understand the physical meaning of the natural frequency in Eq. (53), consider a RPV blocked system (Fig. 1) and assume that the pipe with length l_2 (representing the blockage) has a very small cross-sectional area ($\alpha = A_2/A \ll 1$) such that the pipe with length l_1 behaves as a reservoir with respect to Pipe 2. At very low frequency such that the wavelength is much greater than l_2 and l_3, the system comprising Pipe 2 and Pipe 3 behaves as a Helmholtz resonator (Stevens 1998, Chapter 3) in which Pipe 2 is equivalent to an acoustic mass (most of the energy in Pipe 2 is kinetic energy) and Pipe 3 is equivalent to an acoustic compliance (most of the energy in pipe 3 is potential energy). Applying the one-dimensional momentum equation (Ghidaoui 2004) in Pipe 2 and assuming an ideal fluid gives the following result:

$$M\frac{dV_2}{dt} = P_0A_2 - (P_0+P)A_2 \Rightarrow \frac{dV_2}{dt} = -\frac{PA_2}{\rho l_2} \tag{54}$$

where V_2 = velocity in Pipe 2; P = transient pressure; P_0 = pressure at the reservoir; and ρ = density. Applying the continuity equation (Ghidaoui 2004) in Pipe 3 and using the continuity of flow at the junction between Pipe 2 and Pipe 3 $A_2V_2 = A_3V_3$ gives

$$\frac{dM_3}{dt} = \rho V_2A_2 \Rightarrow \frac{d\rho A_3 l_3}{dt} = \rho V_2A_2 \tag{55}$$

where V_3 = velocity in Pipe 3; and l_3 = length of Pipe 3. Using the state equation $dP/d\rho = a^2$ yields

$$\frac{dP}{dt} = \alpha a^2\frac{\rho}{l_3}V_2 \Rightarrow \frac{d^2P}{dt^2} = \alpha a^2\frac{\rho}{l_3}\frac{dV_2}{dt} \tag{56}$$

Inserting Eq. (54) into Eq. (56), gives

$$\frac{d^2P}{dt^2} - \frac{a^2}{L^2}\frac{\alpha}{\eta_3\eta_2}P = 0 \tag{57}$$

which is the ordinary differential equation of a Helmholtz resonator system with natural frequency (w_H)

$$w_H = \frac{a}{L}\sqrt{\frac{\alpha}{\eta_3\eta_2}} \Rightarrow \frac{w_H}{w_1^0} = \frac{2}{\pi}\sqrt{\frac{\alpha}{\eta_3\eta_2}} \tag{58}$$

This is identical to Eq. (53). For the short blockage case (Fig. 4), the shift is almost always nearly zero at the lowest mode ($m = 1$). Therefore, a significant shift of the lowest eigenfrequency is a good indication of severe blockage case where Eq. (53) could become an accurate approximation.

Conclusions

The eigenfrequency shift from an interior blockage in a conduit is investigated with the goal being to understand and describe the mechanisms that cause such eigenfrequency shift. This understanding provides insights essential to improving the accuracy and the convergence of inverse techniques for TBDDM and cross-sectional pipe condition assessment.

The variation in eigenfrequency shift caused by a shallow blockage (i.e., small radial protrusion) in a conduit is analyzed by studying the variation of the work done by radiation pressure at the blockage boundaries. In particular, if the work done at one end of a blockage is equal in magnitude and sign to the work done at the other end, then the eigenfrequency shift is zero. This case occurs under two conditions:

1. The blockage length is a multiple of half the wavelength of the mth mode harmonic. At these modes, the eigenfrequency corresponds to the Bragg resonance frequency of total transmission. Under this condition, the shift is zero for any blockage location.
2. At a given mode m, the shift is zero when the blockage midlength is located at a position of equal pressure and flow magnitudes.

On the other hand, maximum shift occurs if the work done by radiation pressure at one blockage boundary is equal in magnitude and opposite in sign to the work done at the other boundary. Two mechanisms govern the maximum shift:

1. For a given mode m, the shift is maximum if the blockage midlength is located at a position of either a pressure node or stagnation point; and
2. For a given mode number, the largest shift magnitude occurs at modes with an eigenfrequency close to the Bragg resonance frequencies of maximum reflection.

Positive and negative shifts depend on which blockage boundaries experience higher work done by radiation pressure. The assumption of shallow blockage applies when the blockage occupies 35% or less of the pipe's area.

For the case of severe and moderate blockage, the blockage locations of zero shift and maximum shift vary with the radial protrusion of the blockage (α). The more severe the blockage, the more

J. Hydraul. Eng., 2018, 144(1): 04017055

these locations are shifted. However, the variation of these locations with respect to the shallow blockage case becomes very small at high modes ($m > 3$). The magnitude of positive shifts is small at low modes and becomes high at modes with eigenfrequencies close to the Bragg resonance frequency of maximum reflection. When such a significant positive shift is measured, it provides an accurate estimate of the Bragg resonance frequency from which the blockage characteristics can be determined. The first eigenfrequency can be well approximated by the natural frequency of a Helmholtz resonator system. The conclusion and results in this work are studied experimentally in Louati et al. (2017).

Appendix. Hessian Matrix for Positive and Negative Maximum Shifts

$$\mathbf{D}_H = \frac{\partial^2\left(\frac{\overline{\Delta w_m}}{w_1^0}\right)}{\partial(\eta_3+\frac{\eta_2}{2})^2}\frac{\partial^2\left(\frac{\overline{\Delta w_m}}{w_1^0}\right)}{\partial(\eta_3)^2} - \frac{\partial^2\left(\frac{\overline{\Delta w_m}}{w_1^0}\right)}{\partial(\eta_3+\frac{\eta_2}{2})\partial(\eta_3)} \tag{59}$$

with

$$\frac{\partial^2\left(\frac{\overline{\Delta w_m}}{w_1^0}\right)}{\partial(\eta_3+\frac{\eta_2}{2})^2} = -\frac{(1-\alpha)}{\pi}[(2m-1)\pi]^2\begin{Bmatrix} 2\sin\left[(2m-1)\frac{\pi}{2}\eta_2\right] \\ \cos\left[(2m-1)\pi\left(\eta_3+\frac{\eta_2}{2}\right)\right]\end{Bmatrix}$$

$$\frac{\partial^2\left(\frac{\overline{\Delta w_m}}{w_1^0}\right)}{\partial(\eta_2)^2} = -\frac{(1-\alpha)}{\pi}\left[(2m-1)\frac{\pi}{2}\right]^2\begin{Bmatrix} 2\sin\left[(2m-1)\frac{\pi}{2}\eta_2\right] \\ \cos\left[(2m-1)\pi\left(\eta_3+\frac{\eta_2}{2}\right)\right]\end{Bmatrix}$$

$$\frac{\partial^2\left(\frac{\overline{\Delta w_m}}{w_1^0}\right)}{\partial(\eta_3+\frac{\eta_2}{2})\partial(\eta_3)} = -\frac{(1-\alpha)}{2\pi}[(2m-1)\pi]^2\begin{Bmatrix} 2\cos\left[(2m-1)\frac{\pi}{2}\eta_2\right] \\ \sin\left[(2m-1)\pi\left(\eta_3+\frac{\eta_2}{2}\right)\right]\end{Bmatrix} \tag{60}$$

which at the critical points conditions [Eq. (12)] gives

$$\mathbf{D}_H = \left[\frac{(1-\alpha)}{\pi}\right]^2[(2m-1)\pi]^4(-1)^{2(\bar{m}+\overline{m'}+1)} > 0 \tag{61}$$

with

$$\frac{\partial^2\left(\frac{\overline{\Delta w_m}}{w_1^0}\right)}{\partial(\eta_3+\frac{\eta_2}{2})^2} = -2\frac{(1-\alpha)}{\pi}[(2m-1)\pi]^2(-1)^{\bar{m}+\overline{m'}+1}$$

$$\frac{\partial^2\left(\frac{\overline{\Delta w_m}}{w_1^0}\right)}{\partial(\eta_2)^2} = -2\frac{(1-\alpha)}{\pi}\left[(2m-1)\frac{\pi}{2}\right]^2(-1)^{\bar{m}+\overline{m'}+1}$$

$$\frac{\partial^2\left(\frac{\overline{\Delta w_m}}{w_1^0}\right)}{\partial(\eta_3+\frac{\eta_2}{2})\partial(\eta_3)} = 0 \tag{62}$$

Acknowledgments

The authors thank Dr. D.A. McInnis for the technical and editorial suggestions. This study is supported by the Hong Kong Research Grant Council (Projects 612712, 612713, and T21-602/15R) and by the Postgraduate Studentship.

Notation

The following symbols are used in this paper:

A_0 = area of intact pipe (m^2);
A_2 = area of pipe with reduced cross-sectional area (m^2);
a = acoustic wave speed in water (ms^{-1});
g = acceleration due to gravity ($m\,s^{-2}$);
h_m^{amp} = mth maximum complex amplitude of pressure head (m);
i = $\sqrt{-1}$;
k_m^{max} = mth wavenumber at maximum shift ($rad\,m^{-1}$);
L = whole pipe length (m);
l_1 = length of Pipe 1 (m);
l_2 = length of Pipe 2 (m);
l_3 = length of Pipe 3 (m);
m = mode number for pipe system of length L;
n_T = integer that gives the number of modes region between two consecutive Bragg resonance frequencies of total transmission;
P = pressure (Pa);
q_m^{amp} = mth maximum complex amplitude of flow discharge (m);
V_2 = velocity in Pipe 2 ($m\,s^{-1}$);
V_3 = velocity in Pipe 3 ($m\,s^{-1}$);
w_H = natural frequency of Helmholtz resonator system ($rad\,s^{-1}$);
w_m = mth resonant frequencies in the blocked pipe case ($rad\,s^{-1}$);
w_m^0 = mth resonant frequencies in the intact pipe case ($rad\,s^{-1}$);
x = axial coordinate (m);
α = area ratio between the blocked pipe section (A_2) and the intact pipe section (A_0);
Δw_m = mth eigenfrequency shift ($rad\,s^{-1}$);
η_1 = l_1/L dimensionless length;
η_2 = l_2/L dimensionless length;
ξ = counting numbers; and
ρ = density.

References

Beyer, R. T. (1978). "Radiation pressure—The history of a mislabelled tensor." *J. Acoust. Soc. Am.*, 63(4), 1025–1030.
Borgnis, F. E. (1953). "Acoustic radiation pressure of plane compressional waves." *Rev. Modern Phys.*, 25(3), 653–664.
Bragg, W. H., and Bragg, W. L. (1913). "The reflection of X-rays by crystals." *Proc. R. Soc. London, Ser. A*, 88(605), 428–438.
Coelho, B., and Andrade-Campos, A. (2014). "Efficiency achievement in water supply systems—A review." *Renewable Sustainable Energy Rev.*, 30, 59–84.
De Salis, M. H. F., and Oldham, D. J. (1999). "Determination of the blockage area function of a finite duct from a single pressure response measurement." *J. Sound Vib.*, 221(1), 180–186.
Domis, M. A. (1979). "Acoustic resonances as a means of blockage detection in sodium cooled fast reactors." *Nucl. Eng. Des.*, 54(1), 125–147.
Domis, M. A. (1980). "Frequency dependence of acoustic resonances on blockage position in a fast reactor subassembly wrapper." *J. Sound Vib.*, 72(4), 443–450.
Duan, H. F., Lee, P. J., Ghidaoui, M. S., and Tung, Y. K. (2011). "Extended blockage detection in pipelines by using the system frequency response analysis." *J. Water Resour. Plann. Manage.*, 10.1061/(ASCE)WR.1943-5452.0000145, 55–62.
Duan, H. F., Lee, P. J., Kashima, A., Lu, J. L., Ghidaoui, M. S., and Tung, Y. K. (2013). "Extended blockage detection in pipes using the frequency response method: Analytical analysis and experimental verification." *J. Hydraul. Eng.*, 10.1061/(ASCE)HY.1943-7900.0000736, 763–771.

Duan, W., Kirby, R., Prisutova, J., and Horoshenkov, K. V. (2015). "On the use of power reflection ratio and phase change to determine the geometry of a blockage in a pipe." *Appl. Acoust.*, 87, 190–197.
Ehrenfest, P. (1917). "On adiabatic changes of a system in connection with the quantum theory." *KNAW Proc.*, 19, Amsterdam, Netherlands, 576–597.
El-Rahed, M., and Wagner, P. (1982). "Acoustic propagation in rigid ducts with blockage." *J. Acoust. Soc. Am.*, 72(3), 1046–1055.
Fant, G. (1975). "Vocal-tract area and length perturbations." *STL-QPSR 4/1975*, Speech Transmission Laboratory, Dept. of Speech Communication, Royal Institute of Technology, Stockholm, Sweden, 1–14.
Ghidaoui, M. S. (2004). "On the fundamental equations of water hammer." *Urban Water J.*, 1(2), 71–83.
Heinz, J. (1967). "Perturbation functions for the determination of vocal-tract area functions from vocal-tract eigenvalues." *STL-QPSR 1/1967*, Speech Transmission Laboratory, Dept. of Speech Communication, Royal Institute of Technology, Stockholm, Sweden, 1–14.
James, W., and Shahzad, A. (2012). "Water distribution losses caused by encrustation and biofouling: Theoretical study applied to Walkerton, ON." *World Water and Environmental Resources Congress 2003*, ASCE, Reston, VA, 1–10.
Lee, P. J., Duan, H. F., Ghidaoui, M., and Karney, B. (2013). "Frequency domain analysis of pipe fluid transient behaviour." *J. Hydraul. Res.*, 51(6), 609–622.
Lee, P. J., Vítkovský, J. P., Lambert, M. F., Simpson, A. R., and Liggett, J. (2008). "Discrete blockage detection in pipelines using the frequency response diagram: Numerical study." *J. Hydraul. Eng.*, 10.1061/(ASCE)0733-9429(2008)134:5(658), 658–663.
Louati, M. (2013). "On wave-defect interaction in pressurized conduits." *Proc., 35th IAHR Congress*, International Association for Hydraulic Research, Chengdu, China.
Louati, M. (2016). "In-depth study of plane wave-blockage interaction and analysis of high frequency waves behaviour in water-filled pipe systems." Ph.D. dissertation, Hong Kong Univ. of Science and Technology, Hong Kong.
Louati, M., and Ghidaoui, M. S. (2015). "Role of length of probing waves for multi-scale defects detection." *Proc., 36th IAHR World Congress*, International Association for Hydraulic Research, The Hague, Netherlands.
Louati, M., and Ghidaoui, M. S. (2016). "In-depth study of the eigenfrequency shift mechanism due to variation in the cross-sectional area of a conduit." *J. Hydraul. Res.*, in press.
Louati, M., Ghidaoui, M. S., Meniconi, S., and Brunone, B. (2016). "Bragg-type resonance in blocked pipe system and its effect on the eigenfrequency shift." *J. Hydraul. Eng.*, in press.
Louati, M., Meniconi, M., Ghidaoui, M. S., and Brunone, B. (2017). "Experimental study of the eigenfrequency shift mechanism in blocked pipe system." *J. Hydraul. Eng.*, 10.1061/(ASCE)HY.1943-7900.0001347, 04017044.
Mei, C. C. (1985). "Resonant reflection of surface waves by periodic sandbars." *J. Fluid Mech.*, 152(-1), 315–335.
Meniconi, S., Duan, H. F., Lee, P. J., Brunone, B., Ghidaoui, M. S., and Ferrante, M. (2013). "Experimental investigation of coupled frequency and time-domain transient test-based techniques for partial blockage detection in pipelines." *J. Hydraul. Eng.*, 10.1061/(ASCE)HY.1943-7900.0000768, 1033–1040.
Mermelstein, P. (1967). "Determination of the vocal-tract shape from measured formant frequencies." *J. Acoust. Soc. Am.*, 41(5), 1283–1294.
Milenkovic, P. (1984). "Vocal tract area functions from two point acoustic measurements with formant frequency constraints." *Acoust. Speech Signal Proc. IEEE Trans.*, 32(6), 1122–1135.
Milenkovic, P. (1987). "Acoustic tube reconstruction from noncausal excitation." *IEEE Trans. Acoust. Speech Signal Process.*, 35(8), 1089–1100.
Mohapatra, P. K., Chaudhry, M. H., Kassem, A. A., and Moloo, J. (2006). "Detection of partial blockage in single pipelines." *J. Hydraul. Eng.*, 10.1061/(ASCE)0733-9429(2006)132:2(200), 200–206.
Qunli, W., and Fricke, F. (1989). "Estimation of blockage dimensions in a duct using measured eigenfrequency shifts." *J. Sound Vib.*, 133(2), 289–301.
Qunli, W., and Fricke, F. (1990). "Determination of blocking locations and cross-sectional area in a duct by eigenfrequency shifts." *J. Acoust. Soc. Am.*, 87(1), 67–75.
Sattar, A. M., Chaudhry, M. H., and Kassem, A. A. (2008). "Partial blockage detection in pipelines by frequency response method." *J. Hydraul. Eng.*, 10.1061/(ASCE)0733-9429(2008)134:1(76), 76–89.
Schroeder, M. R. (1967). "Determination of the geometry of the human vocal tract by acoustic measurements." *J. Acoust. Soc. Am.*, 41(4B), 1002–1010.
Schroeter, J., and Sondhi, M. M. (1994). "Techniques for estimating vocal-tract shapes from the speech signal." *Speech Audio Proc. IEEE Trans.*, 2(1), 133–150.
Sondhi, M. M., and Gopinath, B. (1971). "Determination of vocal- tract shape from impulse response at the lips." *J. Acoust. Soc. Am.*, 49(6B), 1867–1873.
Sondhi, M. M., and Resnick, J. (1983). "The inverse problem for the vocal tract: Numerical methods, acoustical experiments, and speech synthesis." *J. Acoust. Soc. Am.*, 73(3), 985–1002.
Stevens, K. N. (1998). *Acoustic phonetics*, MIT Press, Cambridge, MA.
Wang, X. J., Lambert, M. F., and Simpson, A. R. (2005). "Detection and location of a partial blockage in a pipeline using damping of fluid transients." *J. Water Resour. Plann. Manage.*, 10.1061/(ASCE)0733-9496(2005)131:3(244), 244–249.